ACS OMEGA

http://pubs.acs.org/journal/acsodf

Article

Sulfide (H_2S) Corrosion Modeling of Cr-Doped Iron (Fe) Using a Molecular Modeling Approach

Mohammad Asif, Faisal Khan,* Kelly Hawboldt, and Shams Anwar

Cite This: *ACS Omega* 2023, 8, 7395−7406

Read Online

ACCESS | Metrics & More | Article Recommendations

ABSTRACT: This work presents the use of density functional theory to study the adsorption/dissociation mechanism of the H_2S molecule at the Cr-doped iron (Fe(100)) surface. It is observed that H_2S is weakly adsorbed on Cr-doped Fe; however, the dissociated products are strongly chemisorbed. The most feasible path for disassociation of HS is favorable at Fe compared to Cr-doped Fe. This study also shows that H_2S dissociation is a kinetically facile process, and the hydrogen diffusion follows the tortuous path. This study helps better understand the sulfide corrosion mechanism and its impact, which would help design effective corrosion prevention coatings.

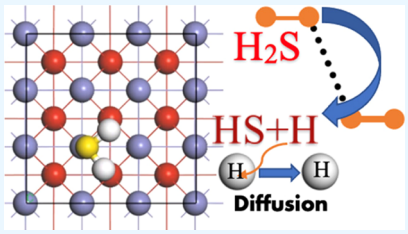

1. INTRODUCTION

Steel containing Cr, an iron alloy produced from iron, is widely used to transport crude oil and gas due to its ductility, excellent stress absorbing abilities, and cost-effectiveness. However, iron loses its mechanical properties in acidic environments[1−3] as the iron crystal acts as an electron conductor resulting in corrosion. In the oil and gas industry, corrosion is typically found in pipelines and the process equipment.[4] Pipelines are crucial for long-distance transportation of crude oil and natural gas at a low cost and are capable of handling large volumes.[5]

The consequences of corrosion include increased maintenance and operating costs, breakdowns, and failures.[6] In 2015, corrosion losses at the global level amounted to $US 2.5 trillion.[7] Corrosion can take many forms including biocorrosion where microorganisms present at the metal surface combined with environmental conditions impact the corrosion rate.[8] An estimated 20% of the annual losses is attributed to microbiologically influenced corrosion.[9,10]

The electrochemical reactions associated with biocorrosion occur in the biofilm[11] in which microorganisms stick to the surface. The possible reactions in the biofilm at the metal surface include electron transfer between species such as H_2S, S^{2-}, Fe^{2+}, FeS, SO_4^{2-}, H_2O, CO_2, and Cl^-. Hydrogen sulfide (H_2S), carbon dioxide (CO_2), and chloride ions (Cl^-) are highly corrosive and have the potential to rapidly degrade petroleum equipment in humid environments, seriously compromising the safety and reliability of these systems.[12] H_2S is generated via a number of mechanisms; however, sulfate-reducing bacteria are the primary source in seawater-injected oil and gas fields and sewage systems.[13] H_2S is capable of widespread corrosion, local corrosion, and pitting corrosion of many metals.[14,15] Shoesmith et al.[16] studied the electrochemical behavior of iron in alkaline sulfide solutions.

Natural protection against corrosion can be achieved by either alloying the metal or the formation of a metal oxide layer on the surface. The Fe_2O_3 and Fe_3O_4 layers provide enough protection in a mild corrosive environment (<500 °C). If the temperature rises or the environment becomes more corrosive, other steel grades may be employed or another coating was applied.[17] Several different oxide layers, composed of Cr_2O_3, Ni_2O_3, and Mn_3O_4, provide corrosion resistance to the steel.[18,19] An oxide layer is formed when sulfide is not present as the presence of sulfur inhibits oxide growth. With sufficient anodic potential, the oxide layer II is attacked, producing ferric sulfide because of a breakdown in passivity. By oxidizing the sulfide ion, a deposit of elemental sulfur is formed on the electrodes. Levy and Yong-Fa[20] reported that the most significant surface degradation mechanism was formed by the erosion of oxide scale on a steel surface. Analyzing the adsorption phenomenon of corrosion products (HS, S, hydrogen) can give the means to explore the subsequent reactions occurring in the presence of H_2S. Das et al.[21] studied anisotropic structure of H_2S with the help of microwave spectroscopy. They found that (H_2S) will also form a hydrogen-bonded system like water.

High-chromium alloys provide better protection than simple iron steel at higher temperatures and in more aggressive conditions. These include ferrite steel alloys, austenitic steel alloys, and ferritic high alloy steels. In the case of steels with chromium, there was a significant difference between the scale loss mechanism, for instance steels with Cr between 5 and 9 wt % Cr lose metal at a much lower rate than steels below 5 wt %

Received: August 31, 2022
Accepted: January 3, 2023
Published: February 15, 2023

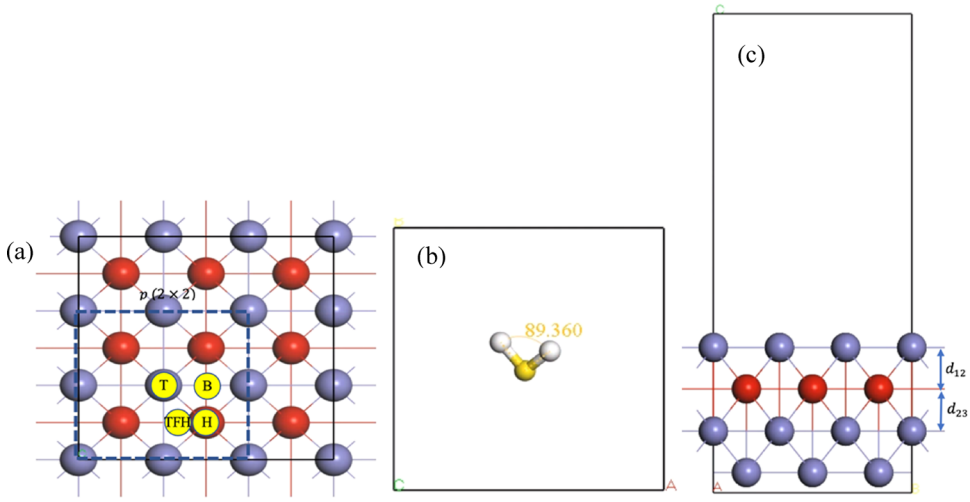

Figure 1. (a) Four kinds of sites at the surface; T (top), B (bridge), H (hollow), and TFH (threefold hollow) are shown with respect to locations, (b) free H_2S molecule, and (c) side view of free slab with d_{12} is the distance between layers 1 and 2; d_{23} is the distance between layers 2 and 3. Second-layer Fe atoms are red in color. Fe Fe S H Cr

Cr. However, the morphology of the ferritic steel scales is a more important factor than the composition in the rate of metal loss. Cr helps to decrease scale formation and removal, as well as metal loss through scale formation and removal when it is present in the austenitic steel scales. There is a correlation between the drop-in corrosion rate and abnormal surface segregation of Cr resulting from the complex interaction between atoms in bulk and surfaces.[22−25] The corrosion behavior of steel containing Cr is significant for understanding the passivation effect in the presence of strong oxidizing elements/compounds.

The mechanism of reactions that occurs at Fe/S/H_2S interfaces is central to sulfide corrosion processes in an acidic environment.[26] The environment is acidified by H_2S, and steel pipes are pitted. The corrosion contributing reactions in H_2S systems are[27]

H_2S reduction:

$$2H_2S(aq) \rightarrow 2H^+(aq) + 2HS^-(aq) + 2e^-$$

HS^- dissolution:

$$HS^-(aq) \leftrightarrow H^+(aq) + S^{2-}(aq)$$

FeS formation by precipitation:

$$Fe(s) + S^{2-}(aq) \leftrightarrow FeS(s) + 2e^-$$

Recently due to advancement in computational power, density functional theory (DFT) has been used as a tool to estimate reaction parameters such as activation energy barrier, heat of reaction, and structural parameters.[28]

In an atomistic level study,[29] the electronics and structural properties of oxygen adsorptions on Fe(100) and Fe(110) surfaces were investigated. Studies from Błoński et al.,[30] Tan et al.,[31] and Ossowski and Kiejna[32] investigated the effect of oxygen coverage (passivation effect) on electronic and magnetic properties for low-index surfaces such as Fe(100) and Fe(110). Adsorption and dissociation mechanisms of H_2S at FeS, Rh(100), and Fe(110)[26,33,34] are well studied from the DFT.

The corrosion of iron doped with Cr has attracted considerable attention in scientific literature[35−38] in part as it is an economically important material. There is a lack of atomic-level knowledge of how the sulfide layer forms on Fe−Cr surfaces and the process of oxidation. Computational studies have primarily investigated cases of pure Cr and Fe in the initial oxidation process. Yuan et al.[39] investigated the effect of segregating alloying elements on oxygen adsorption on Fe(100) surfaces employing DFT with generalized gradient approximation (GGA).

In this paper, adsorption/dissociation of H_2S on Cr-doped Fe(100) is performed using DFT. The findings (adsorption characteristic, reaction parameters, diffusion of hydrogen) of Cr-doped Fe(100) surfaces are compared with those of the pure iron. The adsorption occurs at the sites namely top (T), bridge (B), and hollow (H) shown in Figure 1. There are a number of reaction paths; however, in this paper, dissociation from the most stable sites T at Fe(100) and B at Cr-doped Fe(100) is considered. A number of diffusional paths for hydrogen on the surface and subsurface (bulk) between a wide range of sites are estimated to understand the embrittlement problems in alloys. These microscale findings will help to protect iron/alloy from corrosion in real operational condition.

2. MOLECULAR MODEL DEVELOPMENT

This study has adopted the DFT approach with the generalized gradient approximation with the Perdew−Burke−Ernzerhof (GGA-PBE)[40] function using the DMol3[41] module in BIOVIA materials studio 2017 software. Dmol3 includes either a Fermi occupation scheme (electronic occupation scheme suitable for covalent bonded system) or a thermal occupation procedure (to compute fractional occupation of orbitals suitable for metallic systems), which is sometimes necessary for converging electronic density.[42]

The four-layer Fe(100) surfaces with a 3 × 3 supercell with 36 atoms were used for the first-principle calculations. The four-layer model is well tested and used widely for quantum calculations.[43,44] The vacuum for the slab was set to 14 Å in the direction normal to the sheet for sufficient space between two cleaved surfaces, such that they did not interact with each other.

A double numerical plus polarization (DNP) was used as a basis set (representation of electronic wave function), which employs a d-type polarization function to heavier atoms (Fe,

https://doi.org/10.1021/acsomega.2c05615
ACS Omega 2023, 8, 7395−7406

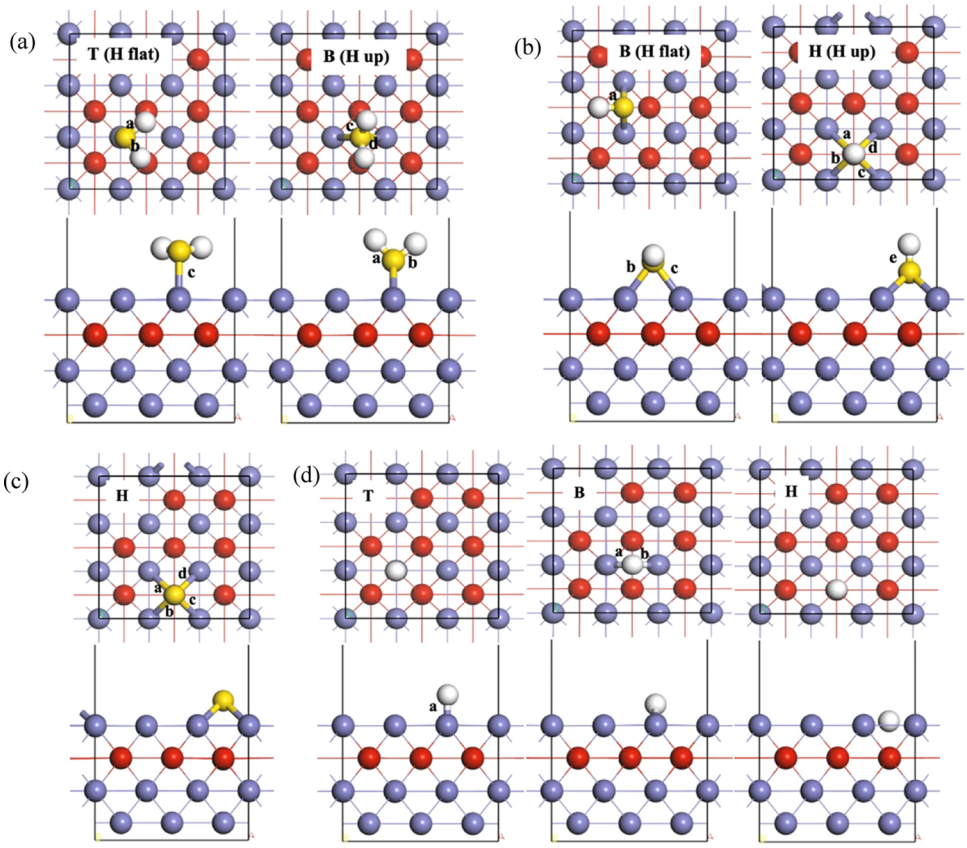

Figure 2. Top view and side view of the optimized geometries for the stable adsorption for (a) H_2S (b) HS (c) S, and (d) hydrogen at Fe(100). T is the top site; B is the bridge site, and H is the hollow site. The H in bracket corresponding to hydrogen atom orientation such as B (H up) is the bridge site with hydrogen atom facing upward direction. The bond length for H−S, Fe−S, and Fe−H are indicated with alphabets a, b, and c. The values are shown in Appendix Table A5. Second-layer Fe atoms are red in color. Fe Fe S H Cr

Cr) and p-type polarization functions to hydrogen atoms; this gives better accuracy than Gaussian 6-31G(d,p).[45] The DNP corresponding to the double zeta quality basis set has comparable or less basis set superposition error (BSSE) than Gaussian 6-31G(d,p).[46] To ensure the accuracy of the model, we performed a convergence test for the total ground-state energy of the Fe(100) with varying k point using different basis sets. The total ground-state energy is shown in Appendix Tables A3 and A4. For the selection of k point from Table A3, we chose to mesh size 3 × 3 × 1 as a balanced option (between computational cost and precision of results) given 2 × 2 × 1 and 4 × 4 × 1 have similar energy levels.

All the atoms were allowed to relax until convergence in cut off energy, force, and displacement reached to 1×10^{-5} Ha (2.72×10^{-4} eV),0.004 Ha/Å (0.1088 eV/Å) and 0.005 Å, respectively. In all calculations, Grimme density function dispersion correction (DFT-D) is applied.[47]

The slab is optimized using the spacing of 16 × 16 × 16 for bulk iron and 3 × 3 × 1 for surface (with adsorbate) of Monkhorst−Pack for k-point Brillouin zone sampling.[48] The calculated lattice constant for BCC iron (took from software directory) was $a = b = c = 2.860$ Å after optimization in excellent agreement to the experimental value of 2.866 Å.[49]

The adsorption energy of reactants/products is calculated by the following expression[50]

$$E_{ad} = -[E_{R/P(slab)} - (E_{slab} + E_{R/P})]$$

where $E_{R/P(slab)}$ is the energy of reactants/products in binding state, E_{slab} is the energy of the slab, and $E_{R/P}$ is the energy of the reactants/product in free state.

The relaxation between layers is calculated by the following:[51]

$$\Delta_{ij} = \frac{d_{ij}(\text{ad}) - d_{ij}(\text{bulk})}{d_{ij}(\text{bulk})}$$

where Δ_{ij} is the relaxation between i and j layers of the Fe(100) slab, d_{ij}(ad) the distance between i and j layers of the Fe(100) slab when species is adsorbed (can be seen in Figure 1c), and d_{ij}(bulk) is the distance between i and j layers of an Fe(100) slab without any adsorption. Positive/negative values of relaxation between first and second layers (Δ_{12}) indicate that the surface moves outward/inward (compared with bulk) after geometric optimization.

The activation energy barriers (E_a) and the reaction energy (ΔE) for dissociation of $H_2S \rightarrow HS + H \rightarrow S + 2H$ are defined as follows:[52]

$$E_a = E_{TS} - E_{IS}$$

$$\Delta E = E_{FS} - E_{IS}$$

where E_{TS} is the energy of the transition state, E_{IS} is the energy of the initial state, and E_{FS} is the energy of the final state.

The transition state (TS) for all reaction/diffusion pathways is performed by the nudge elastic band (NEB) method. This method works on optimizing several images along the reaction

https://doi.org/10.1021/acsomega.2c05615
ACS Omega 2023, 8, 7395−7406

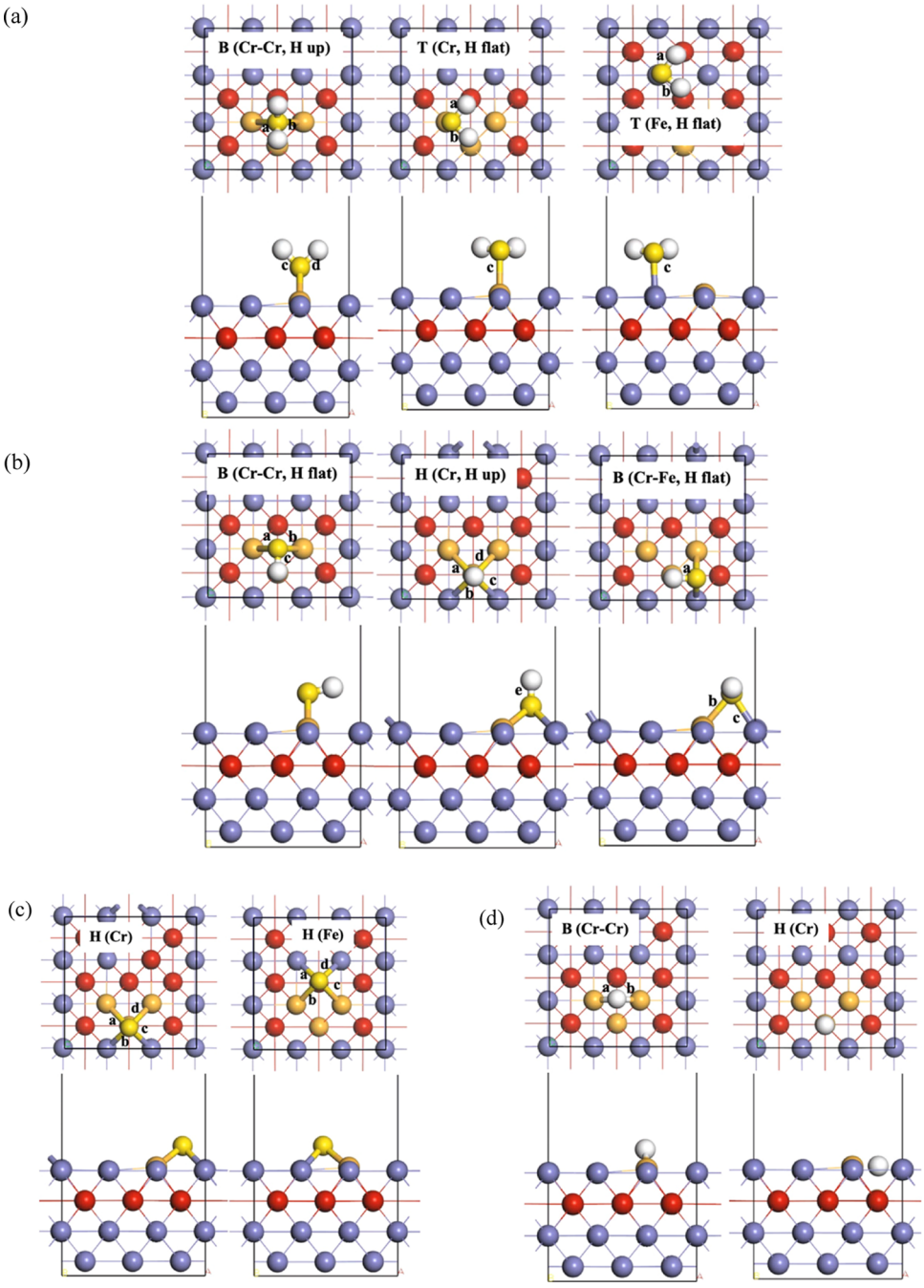

Figure 3. Top view and side view for optimized geometries for stable adsorption for (a) H_2S (b) HS (c) S, and (d) hydrogen for Cr-doped Fe(100). T is the top site; B is the bridge site, and H is the hollow site. The H in bracket corresponds to hydrogen atom orientation such as B (H up) is the bridge site with hydrogen atom facing upward direction. The bond length for H−S, Fe−S, and Fe−H are indicated with alphabets a, b, and c. The values are shown in Appendix Table A6. Second-layer Fe atoms are red in color. Fe Fe S H Cr

paths. The run is repeated until the stationary point is reached.[53] To confirm the minimum energy pathway, we used the TS confirmation tool available in the DMol3.

3. RESULTS AND DISCUSSION

3.1. Adsorption of Reactants and Products. Hu et al.[57] studied the adsorption behavior of H_2O, H^+, Cl^-, and OH^- on the clean and Cr-doped Fe(110). In their work, only one Fe atom is replaced with Cr. In this work, three Fe atoms are replaced with Cr (7.8 wt %) at Fe(100) as the corrosion rate in alloy steel drops rapidly as Cr content approaches 8%.[58] The calculation of Cr wt % is shown in Appendix. The Fe atom can be replaced with the Cr atom via (i) random replacement, (ii) replacing the second layer iron atoms, (iii) replacing the combination of the first layer and second layer iron atoms, and (iv) replacing only the top layer atoms. For this work, replacement scheme (iii), in which Cr atoms are accumulated, is chosen based on minimum ground state energy. A study done by Bradley[59] also shows, at low temperature atoms of similar kind stay together; however, at higher temperature this trend disappears.

https://doi.org/10.1021/acsomega.2c05615
ACS Omega 2023, 8, 7395−7406

Table 1. Adsorption Energy and Geometric Parameters for the Adsorption of Reactants and Products at the Fe(100)[a]

species	adsorption site	d (surf-S)/Å	d (S−H)/Å	$Ø_{HSH}$/°	$-E_{ad}$/eV	Δ_{12}/%	Δ_{23}/%
H_2S	T (H flat)	2.310 (2.422)[c]	1.437, 1.455 (1.431)[c]	89.222 (89.167)[c]	0.999 (0.763)[c]	−0.782	2.078
	B (H up)	1.891	1.426, 1.427	94.791	0.947	−0.112	3.335
HS	B (H flat)	1.931 (2.326)[d]	1.429 (1.361)[d]		4.457 (3.60)[d]	−0.168	3.335
	H (H up)	1.367 (2.343)[d]	1.438 (1.385)[d]		4.329 (3.98)[d]	−0.503	2.679
S	H	1.419			6.661 (6.87)[b]	−0.782	2.242
hydrogen	T	1.685			2.357 (2.21)[e]	−0.056	0.164
	B	1.167			2.659 (2.71)[e]	0.000	0.711
	H	0.212			2.610 (2.68)[e]	−0.056	0.164

[a] d (surf-S)/Å is the distance of sulfur atom from the surface. d (S−H)/Å is the bond length of S−H, $Ø_{HSH}$ (°) is the angle between hydrogen atoms in H_2S, E_{ad} (eV) is the adsorption energies, Δ_{12} (%) is the relaxation between first and second layer, and Δ_{23} (%) is the relaxation between second and third layer. [b] Ref 54. [c] Ref 55. [d] Ref 56. [e] Ref 44.

Table 2. Adsorption Energy and Geometric Parameters for the Adsorption of Reactants and Products at Cr-Doped Fe(100)[a]

species	adsorption site	d (surf-S)/Å	d (S−H)/Å	$Ø_{HSH}$/°	$-E_{ad}$/eV	Δ_{12}/%	Δ_{23}/%
H_2S	B (Cr−Cr, H up)	2.150	1.421, 1.422	94.637	0.967	−0.055	0.167
	T (Cr, H flat)	2.443	1.428, 1.513	88.905	0.917	−0.829	0.835
	T (Fe, H flat)	2.343	1.429, 1.455	89.584	0.944	−0.774	1.169
HS	B (Cr−Cr, H flat)	2.151	1.429		4.400	−0.332	0.612
	H (Cr, H up)	1.464	1.432		4.346	−0.608	0.056
	B (Cr−Fe, H flat)	2.055	1.437		4.398	−0.106	0.445
S	H (Cr)	1.475			6.688	−0.719	0.445
	H (Fe)	1.504			6.682	−0.663	0.390
hydrogen	B (Cr−Cr)	1.405			2.651	−0.387	0.947
	H (Cr)	0.208			2.689	−0.111	0.501

[a] d (surf-S)/Å is the distance of sulfur atom from the surface. d (S−H)/Å is the bond length of S−H, $Ø_{HSH}$ (°) is the angle between hydrogen atoms in H_2S, E_{ad} (eV) is the adsorption energies. Δ_{12} (%) is the relaxation between first and second layer and Δ_{23} (%) is the relaxation between second and third layer.

The most stable adsorption state of the individual component at Fe(100) and Cr-doped Fe(100) surfaces must be established before the disassociation can be modeled. In this work, many adsorption locations/orientation of components were analyzed, such as (i) adsorption over the Fe or Cr (ii) hydrogen atom orientation (flat, upward, or downward) but only a few sites led to the feasible optimization shown in Figures 2 and 3.

The adsorption energy for Fe(100) and Cr-doped Fe(100) is shown in Tables 1 and 2. The microadsorption mechanism can be seen by calculating the bond length, distance from the surface, and angle between hydrogen atoms at these surfaces.

The most stable adsorption of H_2S occurs at the top (H flat) shown in Figure 2a; and the least stable adsorption is the bridge (H up) at the Fe(100) surface. The adsorption energy for the most stable adsorption of H_2S at Fe(100) is found to be 0.999 eV. Ren et al.[55] reported the adsorption energy range of 0.461−2.298 eV for H_2S at various sites. HS adsorbed at location bridge B (H flat) with adsorption energy 4.457 eV at Fe(100). Wen et al.[56] reported adsorption energy for HS as 3.98 eV for the most stable site at Fe(100).

All adsorption energies calculated at the Fe(100) and Cr-doped Fe(100) surfaces are negative, indicating exothermic nature for the reactants and products. This indicates that these species act as corrosive media for Fe(100) and Cr-doped Fe(100). Among H_2S, hydrogen, HS, and S, the adsorption energy of H_2S is the lowest at both Fe(100) and Cr-doped Fe(100) surface, and the adsorption energy of S is the highest among these species. This trend is in good agreement with the previous work.[34,60,61] The mechanism of adsorption is the same for all species at Fe(100) and Cr-doped Fe(100). The H−S bond length for the H_2S at Fe(100) varied from 1.426−1.455 Å and angle varied from $Ø_{HSH}$° of 89.222° − 94.791°, which is in good agreement with Ren et al.[55] They reported that the H−S bond length varied from 1.427−1.491 Å and $Ø_{HSH}$° of 86.071° − 94.696°. The experimental H−S length is 1.328 Å and $Ø_{HSH}$° of 93.556° for the free state of H_2S molecules.[51] The larger bond length further confirms the likelihood of dissociation of H_2S at the Fe(100) surface with a small activation barrier.

For the Cr-doped Fe(100) surface, the most stable adsorption occurs at the B (Cr−Cr, H up) site of H_2S (Figure 3a) with an adsorption energy of 0.967 eV. The H_2S molecule sits at a distance of 2.150 Å (Table 2) at the most stable adsorption for the Cr-doped Fe(100). The adsorption of these species changes the geometric structure of the slab, which can also be observed by the relaxation between layers shown in Tables 1 and 2. It is observed that relaxation between layers significantly decreases for the adsorption of H_2S, HS, S after the addition of Cr atoms into the Fe(100) slab however, for the adsorption of hydrogen atom, the relaxation between layers does not change significantly with addition of Cr. These results are in good agreement with the experiment[62] and other studies shown in Table A1. The S atom is most stable at the H site for Fe(100) and H (Cr) site for Cr-doped Fe(100). Legg et al.[63] confirmed by experiment the S atom prefers to sit on the H site. Placing the S atom at a T site or B site results in the S atom migrating to the H site. The adsorption energy of the S atom for Cr-doped Fe(100) at sites H (Cr) found to be 6.688 eV is highest among species studied in this work.

3.2. Dissociation of H_2S. H_2S disassociation is made up of a series of reactions as the gas dissolves and dissociates into

https://doi.org/10.1021/acsomega.2c05615
ACS Omega 2023, 8, 7395−7406

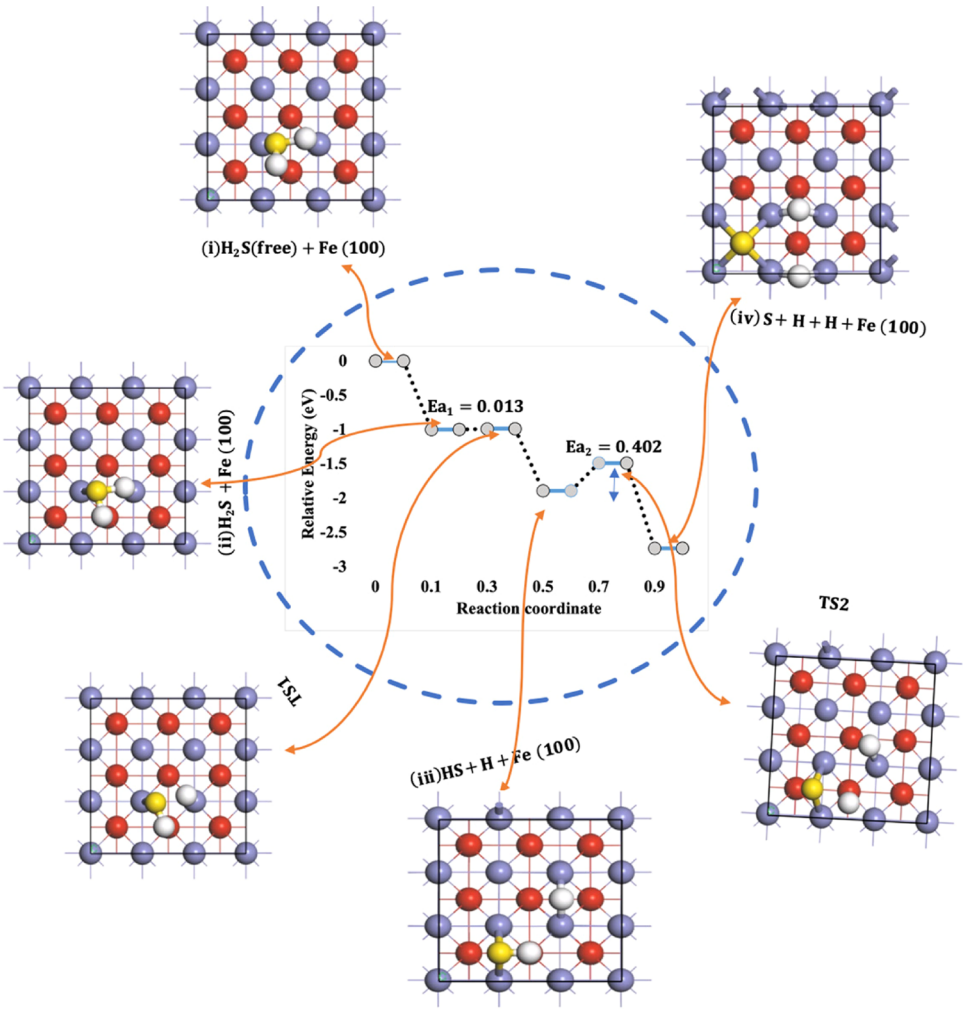

Figure 4. Whole reaction path for the dissociation of H_2S at Fe(100). The top view geometries are shown. Second-layer Fe atoms are red in color. Fe Fe S H Cr

individual components on the metal surface. The decomposition of H_2S at the Fe(100) surface involves a series of reactions:[34]

$$\mathrm{Fe(100)} + \mathrm{H_2S} \rightarrow \mathrm{Fe(100)} + \mathrm{H_2S_{adsorbed}} \quad (1)$$

$$\mathrm{Fe(100)} + \mathrm{H_2S_{adsorbed}} \rightarrow \mathrm{Fe(100)} + \mathrm{HS^-_{adsorbed}} + \mathrm{H^+_{adsorbed}} \quad (2)$$

$$\mathrm{Fe(100)} + \mathrm{HS^-_{adsorbed}} + \mathrm{H^+_{adsorbed}} \rightarrow \mathrm{Fe(100)} + \mathrm{S^{2-}_{adsorbed}} + 2\mathrm{H^+_{adsorbed}} \quad (3)$$

The calculation of transition state (TS) at different sites demonstrates the different dissociation behavior of H_2S is related not only to adsorption energy but also to activation energy (reaction barrier).

The corrosive H_2S gas dissolves to bisulfide (HS) and hydrogen ions with further degradation to hydrogen and S at Fe(100) and Cr-doped Fe(100) surfaces. Previous work on adsorption of H_2S demonstrates that dissociative interactions are thermodynamically favored on Fe_2O_3(001) and at Fe(100),[56,64] The full dissociation process on the Fe(100) slab and Cr-doped Fe(100) slab is shown in Figures 4 and 5 respectively. Dissociation of H_2S can occur from any site but in this work, dissociation is studied from the most stable sites, the T (H flat) at Fe(100) and B (Cr−Cr, H up) at Cr-doped Fe(100). The whole process can be divided into five steps (1) the incoming H_2S gas adsorbs on the stable sites, (2) the adsorbed H_2S gas disassociates to HS and releases one hydrogen atom, (3) the (HS) ion shifts toward the B site for Fe(100) and B (Cr−Cr) site for Cr-doped Fe(100) with a further drop in energy (4) dissociation of (HS) into hydrogen and S by crossing the activation energy barrier at both surfaces, and (5) shift of both hydrogen and S to other stable sites.

By following the trajectory of the reaction process (Figures 4 and 5), it has been observed that the H_2S bond link to the surface slightly rotates and breaks into hydrogen + HS with low activation energy barriers of 0.013 eV for Fe(100) and 0.362 eV at Cr-doped Fe(100). Akande et al.[34] also showed a small dissociation barrier for H_2S at Fe(110), implying easy dissociation of H_2S at iron surfaces. The dissociative adsorption of H_2S is confirmed by X-ray photoelectron spectroscopy,[34,65] from 190 K up to room temperature; however at lower temperatures molecular adsorption occurs. The activation energy barrier for disassociation of HS is 0.402 eV for the Fe(100) and 0.436 eV for the Cr-doped Fe(100), respectively. Wen et al.[56] calculated an activation energy barrier of 0.35 eV for dissociation of HS on an Fe(100) slab. The difference in the activation barrier can be attributed to the distinct path chosen or starting position.

https://doi.org/10.1021/acsomega.2c05615
ACS Omega 2023, 8, 7395−7406

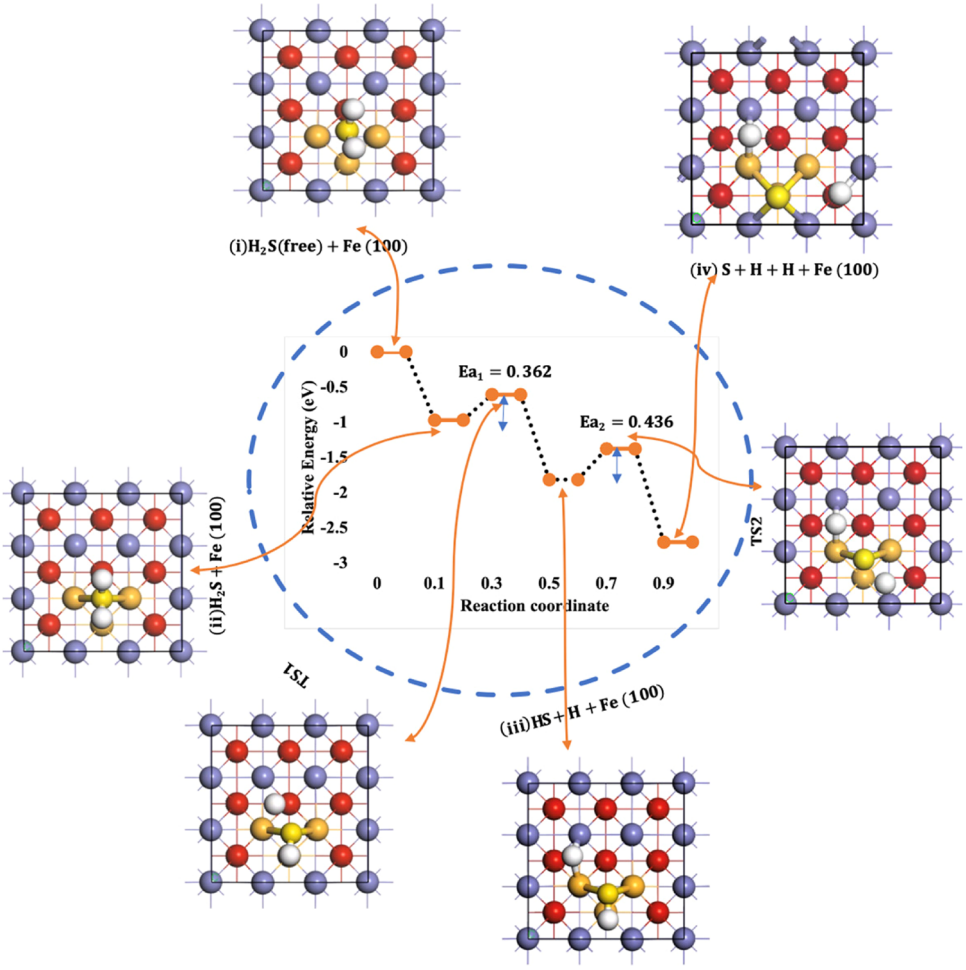

Figure 5. Whole reaction path for the dissociation of H_2S at Cr-doped Fe(100). The top view geometries are shown. Second-layer Fe atoms are red in color. Fe Fe S H Cr

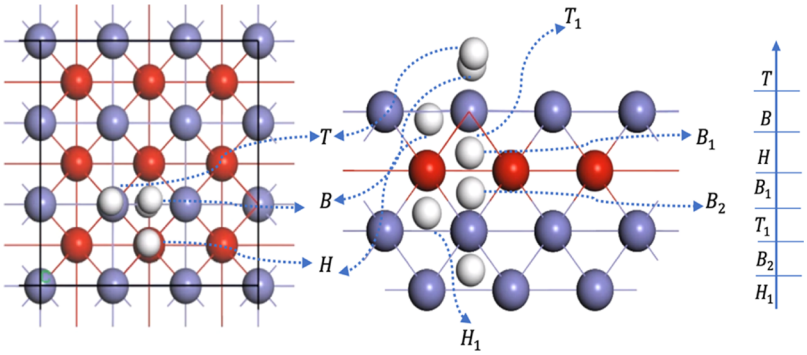

Figure 6. Schematic diagram (top view and side view) of hydrogen atom diffusion sites at the surface and bulk of Fe (100). Fe Fe S H Cr

After dissociation, both hydrogen atoms prefer to sit at a B site; however, the sulfur atom prefers to sit on a H site at Fe(100) (see the final step in Figure 4). The preference of the S atom to sit on the H site at Fe(100) is confirmed by experiment.[63] The first hydrogen atom moves to the B site (Fe−Cr), while the second hydrogen atom sits at a H (above Fe atom); however, the S atom sits at a H site (above Cr) for Cr-doped Fe(100) as depicted in Figure 5.

The dissociation barrier in the Cr-doped Fe(100) slab is higher indicating resistance to the dissociation process. The total energy gain for the (HS + hydrogen) is 1.889 eV at the Fe(100) surface and 1.811 eV at the Cr-doped Fe(100) surface with respect to free molecule (H_2S) after the dissociation process (Figures 4 and 5). Wen et al.[56] reported the total energy gain for HS + hydrogen on the defect-free Fe(100) surface as 1.92 eV.

In Figure 6, three kinds of sites are shown T (top), B (bridge), and H (hollow). The sites in the bulk are B, B_1 is the site below B, and B_2 is the site below B_1 Similarly, T_1 is the site below T. Subscripts 1 and 2 denote bulk locations below the surface sites. Second-layer Fe atoms are red in color. The order of the depths is as follows: T < B < H < B_1 < T_1 < B_2 < H_1.

https://doi.org/10.1021/acsomega.2c05615
ACS Omega 2023, 8, 7395−7406

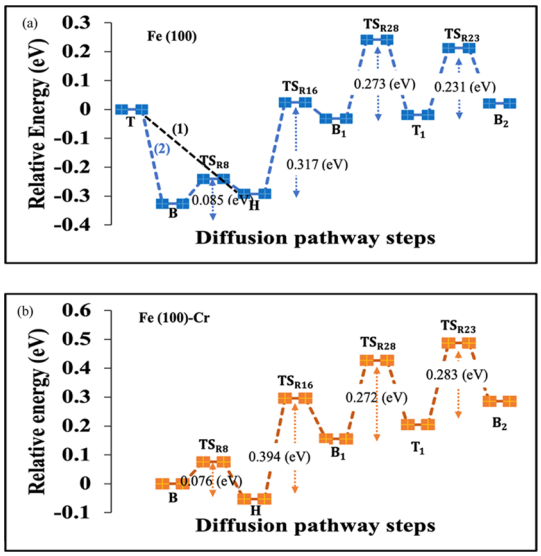

Figure 7. Energy profile of hydrogen atom diffusion at (a) Fe(100) surface via path 1 and 2 (b) Cr-doped Fe(100) surface.

In Figure 7, the curve corresponds to the minimum energy path (MEP) of single hydrogen atom diffusion until the point B_2; however, there are number of paths to reach this point. The arrows indicate a diffusion barrier for hydrogen atoms. TS represents the transition state. R represents routes for which values are taken from Table 3. T and B sites are taken as reference for Fe(100) and for Fe(100)−Cr, respectively.

3.3. Diffusion of Hydrogen. The spontaneous dissociation of H_2S adsorbed at the Fe(100) surface results in two hydrogen atoms. The hydrogen atom diffuses over the surface from the top site to the bridge or hollow site; in addition it also migrates toward the subsurface layer (bulk) of the slab. The effect of the vacancy defect on hydrogen diffusion is discussed by Wen et al.[56] However, the effect of chromium doping of Fe(100) requires study. Therefore, all the feasible routes for MEPs are explored. The activation energy barrier and heat released/absorbed during migration of hydrogen atoms were calculated employing NEB methods. The illustrative diagram for the diffusion of hydrogen among various sites is shown in Figure 6. The four-layer model shown in Figure 6 was symmetrical, so the diffusion of hydrogen atoms was done up to the third inner layer only.

The DFT calculations for hydrogen diffusion over the surface and subsurface give context to hydrogen embrittlement at the microscopic level. Hydrogen diffusion consists of three steps (i) diffusion at the upper surface layer, (ii) dissolution to the lower surface (second layer) at interstitial locations, *and* (iii) diffusion in the bulk Fe(100). There are a large number of energetically stable sites available for dissolution of H atoms in bulk Fe(100), increasing the number of possible diffusion paths. Activation energy E_a (eV) and heat of reaction ΔE (eV) for the diffusion/dissolution of single hydrogen atoms from the various sites at simple Fe(100) slab and Cr-doped Fe(100) slab are shown in Table 3. As noted above, the order of the depths is as follows: T < B < H < B_1 < T_1 < B_2 < H_1. The hydrogen atom can also combine with another hydrogen atom to produce H_2, but this was not considered in this work with respect to diffusion. The diffusion barrier at surface (R_7 : B → H) is 0.085 eV for Fe(100) and 0.076 eV for Cr-doped Fe(100) which is in good agreement with experimental[68] and

Table 3. Activation Energy E_a (eV) and Heat of Reaction ΔE (eV) for the Diffusion of Hydrogen Atoms from Various Sites at the Fe(100) Surface and Cr-Doped Fe(100)

Fe(100)			Fe(100)−Cr		
diffusion routes	ΔE (eV)	E_a (eV)	diffusion routes	ΔE (eV)	E_a (eV)
R_1 : T → B	N/A	N/A	R_1 : T → B	N/A	N/A
R_2: T → H	N/A	N/A	R_2 : T → H	N/A	N/A
R_3 : T → T_1	−0.020	0.385	R_3 : T → T_1	N/A	N/A
R_4 : T → B_1	N/A	N/A	R_4 : T → B_1	N/A	N/A
R_5 : T → B_2	N/A	N/A	R_5 : T → B_2	N/A	N/A
R_6 : T → H_1	N/A	N/A	R_6 : T → H_1	N/A	N/A
R_7 : B → H	0.034	0.085	R_7 : B → H	−0.053	0.076
R_8 : B → T_1	0.307	0.648	R_8 : B → T_1	0.204	0.519
R_9 : B → B_1	0.295	0.423	R_9 : B → B_1	0.155	0.506
R_{10} : B → B_2	0.348	0.781	R_{10} : B → B_2	0.286	0.511
R_{11} : B → H_1	0.306	0.045	R_{11} : B → H_1	N/A	N/A
R_{12} : H → T_1	0.273	0.76	R_{12} : H → T_1	0.257	0.774
R_{13} : H → B_1	0.261	0.317	R_{13} : H → B_1	0.208	0.394
R_{14} : H → B_2	0.313	0.733	R_{14} : H → B_2	−0.339	0.858
R_{15} : H → H_1	N/A	N/A	R_{15} : H → H_1	0.329	1.047
R_{16} : B_1 → T_1	0.012	0.273	R_{16} : B_1 → T_1	0.049	0.272
R_{17} : B_1 → B_2	0.052	0.474	R_{17} : B_1 → B_2	0.130	0.605
R_{18} : B_1 → H_1	0.011	0.531	R_{18} : B_1 → H_1	0.121	0.697
R_{19} : T_1 → B_2	0.040	0.231	R_{19} : T_1 → B_2	0.081	0.283
R_{20} : T_1 → H_1	0.00	0.566	R_{20} : T_1 → H_1	0.072	0.711
R_{21} : B_2 → H_1	−0.041	0.186	R_{21} : B_2 → H_1	−0.009	0.222

other studies shown in Table A2. Out of several possible paths, B → H → B_1 → T_1 → B_2 is chosen (following the minimum activation energy barrier from Table 3) for the hydrogen atom to reach to the site B_2 (third layer). The energy profile of hydrogen atom diffusion is shown in Figure 7. The largest activation energy (steps B → H → B_1 → T_1 → B_2) will be the rate-limiting step for the diffusion of hydrogen atoms to the site B_2. The connection between H → B_1 has the highest barrier, 0.317 eV at Fe(100), and 0.394 eV at Cr-doped Fe(100) and therefore is the rate-limiting step for hydrogen atom diffusion. It is worthwhile noting that hydrogen atoms are not stable at the T site at Cr-doped Fe(100).

The diffusion barrier for R_{11} : B → H_1 at Fe(100) and R_7 : B → H at Cr-doped Fe(100) is the minimum among the paths studied for migration of hydrogen atoms at the surface, implying that the hydrogen atom prefers to diffuse through the B site into the subsurface. The E_a for the first layer diffusion from R_9 : B → B_1 is 0.423 eV and for the Cr-doped Fe(100) from R_9 : B → B_1 is 0.506 eV. Diffusion of the hydrogen atom from R_3 : T → T_1 is exothermic (−0.02 eV); however, R_8 : B → T_1 is endothermic (0.307 eV) at Fe(100).

The diffusion barrier from the H site for R_{12}, R_{13}, R_{14}, and R_{15} at Cr-doped Fe(100) is more than Fe(100), indicating that diffusion of hydrogen atoms from the H site is difficult on Cr-doped Fe(100). The migration of hydrogen atoms at the Fe(100) for the route R_{21} : B_2 → H_1 is preferred compared to a similar path, R_{21} : B_2 → H_1 at the Cr-doped Fe(100) with an activation barrier of 0.186 and 0.222 eV, respectively. Route R_{10} at Fe(100) and R_{15} at Cr-doped Fe(100) has the highest energy barriers of 0.781 and 1.047 eV, respectively (diffusion into the bulk), but the order of E_a (1.047 eV) is low to not inhibit diffusion of the hydrogen atom. The diffusion pathways of hydrogen will clarify the mechanism of embrittlement/hydrogen-induced deterioration.

https://doi.org/10.1021/acsomega.2c05615
ACS Omega 2023, 8, 7395−7406

4. CONCLUSIONS

This study presents understanding of the corrosion mechanism using the GGA-PBE)[40] function with the DMol3[41] module. The corrosion mechanism is studied considering the adsorption mechanism of species H_2S, hydrogen, HS, and S as well as feasible dissociation pathways for Fe(100) and Cr-doped Fe(100). The H_2S is weakly adsorbed for the top (flat hydrogen) site at Fe(100) and bridge (Cr−Cr, hydrogen up) site at Cr-doped Fe(100) with adsorption energies of −0.999 and −0.967 eV, respectively. The most stable adsorption for HS occurs at bridge (hydrogen flat) site for Fe(100) and bridge (Cr−Cr, hydrogen flat) site for Cr-doped Fe(100) with their adsorption energies −4.457 and −4.400 eV respectively. The order of the adsorption energies is $E_{ad}(H_2S) < E_{ad}(H) < E_{ad}(HS) < E_{ad}(S)$ at both surfaces (Fe(100) and Cr-doped Fe(100)), which is in good agreement with previous studies.

The activation energy barrier at Fe(100) for H_2S dissociation is almost negligible; however, for HS dissociation it is 0.402 eV. In addition, the activation energy barrier at Cr-doped Fe(100) for H_2S dissociation is 0.362 eV, and for HS dissociation it is 0.436 eV, respectively. The higher activation barrier for Cr-doped Fe(100) may be due to variable charge density, or the path chosen in this study.

The hydrogen atom diffuses over the surface from the top site to the bridge or hollow site, in addition it also migrates toward the subsurface layer (bulk) of the slab. A large number of diffusion paths are available, but only feasible paths are considered. The diffusion barrier from hollow sites for R_{12}, R_{13}, R_{14}, and R_{15} at Cr-doped Fe(100) is more than Fe(100) shown in Table 3; this implies that the diffusion of hydrogen atoms from the hollow site is difficult in the presence of Cr.

This study will help in understanding the corrosion mechanism due to H_2S for pure metals/alloys. In addition, it will help for investigating the diffusion/formation of H_2 gas inside the bulk (embrittlement) of the metals/alloys.

■ APPENDIX A

Interlayer relaxation for iron; activation energy barrier for diffusion of hydrogen; ground-state energy of Fe(100) for the different k points; ground-state energy of Fe(100) for the different basis sets; bond length for H−S, Fe−S, and Fe−H mentioned in Figure 2 for Fe(100); and bond length for H−S, Fe−S, and Fe−H mentioned in Figure 3 for Cr-doped Fe(100) are presented in Tables A1A2A3A4A5A6.

Table A1. Interlayer Relaxation for Iron[a]

method	layer number	Δ_{12} (%)	Δ_{23} (%)	reference
PAW-GGA (PBE)	4[b]	−0.782	2.078	present work (for most stable sites)
	4[c]	−0.168	3.335	
	4[d]	−0.782	2.242	
	4[e]	0.00	0.711	
PAW-GGA (PBE)	5	−2.2	4.3	51
	7	−2.9	3.0	51
USPP-GGA (PW91)	5	−4.3	3.1	66
	7	−3.8	2.7	66
USPP-GGA (PW91)	5	−3.5	2.3	67
FLAPW-GGA (PBE)	5	−4.0	1.5	68
LEED Experiment		1.4 ± 3		62

[a]Δ_{12} (%) is relaxation between layer 1 and 2, Δ_{23} (%) is relaxation between layer 2 and 3. [b]Adsorption of H_2S on T (H flat) site. [c]Adsorption of HS on B (H flat). [d]Adsorption S on H site. [e]Adsorption hydrogen on B site.

Table A2. Activation Energy Barrier for Diffusion of Hydrogen

metal	temperature range (°C)	experimental method	$-E_{ad}$ (eV)	reference
Fe(100)		DFT	0.085[a]	present work
			0.076[b]	
			0.317[c]	
			0.394[d]	
α-iron	350−900	DFT	0.049	69
	350−700		0.213	
α-iron	126−693	gas phase, time lag	0.047	70
α-iron	25−780	vacuum degassing	0.139	70
carbon steel	10−100	acid attack, time lag	0.399	70

[a]R_7 : B → H at Fe(100). [b]R_7 : B → H at Cr-doped Fe(100). [c]R_{13} : H → B_1 at Fe(100). [d]R_{13} : H → B_1 at Cr-doped Fe(100).

$$\text{Cr . wt \%} = \frac{3\ \text{Cr atom} \times 51.99\ \text{u}}{3\ \text{Cr atom} \times 51.99\ \text{u} + 33\ \text{Fe atom} \times 55.84\ \text{u}} = 7.8\ \%.$$

Table A3. Ground-State Energy of Fe(100) for the Different k Points

k point	basis set	total energy (Ha)
2 × 2 × 1	DNP	45496.726
3 × 3 × 1	DNP	45496.727
4 × 4 × 1	DNP	45496.727

Table A4. Ground-State Energy of Fe(100) for the Different Basis Sets

basis set	total energy (Ha)	DFT-D correction (Ha)
DNP	45496.727	0.318
MIN	45492.937	0.389
DND	45496.723	0.317

Table A5. Bond Length for H−S, Fe−S, and Fe−H Mentioned in Figure 2 for Fe(100)

species	site	A	b	c	d	e
H_2S	T (H flat)	1.437	1.455	2.408		
	B (H up)	1.427	1.426	2.389	2.384	
HS	B (H flat)	1.429	2.415	2.412		
	H (H up)	2.463	2.463	2.462	2.462	1.438
S	H	2.453	2.451	2.452	2.452	
hydrogen	T	1.655				
	B	1.799	1.765			
	H					

https://doi.org/10.1021/acsomega.2c05615
ACS Omega 2023, 8, 7395−7406

Table A6. Bond Length for H−S, Fe−S, and Fe−H Mentioned in Figure 3 for Cr-Doped Fe(100)

species	adsorption site	*a*	*b*	*c*	*d*	*e*
H_2S	B (Cr−Cr, H up)	2.460	2.460	1.422	1.421	
	T (Cr, H flat)	1.513	1.428	2.500		
	T (Fe, H flat)	1.455	1.429	2.418		
HS	B (Cr−Cr, H flat)	2.465	2.465	1.429		
	H (Cr, H up)	2.526	2.459	2.458	2.526	1.432
	B (Cr−Fe, H flat)	1.437	2.470	2.397		
S	H (Cr)	2.506	2.437	2.441	2.510	
	H (Fe)	2.439	2.503	2.503	2.439	
hydrogen	B (Cr−Cr)	1.843	1.845			
	H (Cr)					

AUTHOR INFORMATION

Corresponding Author

Faisal Khan − *Mary Kay O'Connor Process Safety Center (MKOPSC), Artie McFerrin Department of Chemical Engineering, Texas A&M University, College Station, Texas 77843-3122, United States;* orcid.org/0000-0002-5638-4299; Email: fikhan@mun.ca, fikhan@tamu.edu

Authors

Mohammad Asif − *Centre for Risk, Integrity and Safety Engineering (C-RISE) Faculty of Engineering and Applied Science, Memorial University of Newfoundland, St. John's, Newfoundland A1B 3X5, Canada*

Kelly Hawboldt − *Centre for Risk, Integrity and Safety Engineering (C-RISE) Faculty of Engineering and Applied Science, Memorial University of Newfoundland, St. John's, Newfoundland A1B 3X5, Canada*

Shams Anwar − *Centre for Risk, Integrity and Safety Engineering (C-RISE) Faculty of Engineering and Applied Science, Memorial University of Newfoundland, St. John's, Newfoundland A1B 3X5, Canada*

Complete contact information is available at: https://pubs.acs.org/10.1021/acsomega.2c05615

Notes

The authors declare no competing financial interest.

ACKNOWLEDGMENTS

The authors acknowledge the financial support provided by Genome Canada and their supporting partners and the Canada Research Chair (CRC) Tier I Program in Offshore Safety and Risk Engineering.

REFERENCES

(1) Farhadian, A.; Rahimi, A.; Safaei, N.; Shaabani, A.; Abdouss, M.; Alavi, A. A theoretical and experimental study of castor oil-based inhibitor for corrosion inhibition of mild steel in acidic medium at elevated temperatures. *Corros. Sci.* **2020**, *175*, No. 108871.

(2) Corrales-Luna, M.; Le Manh, T.; Romero-Romo, M.; Palomar-Pardavé, M.; Arce-Estrada, E. M. 1-Ethyl 3-methylimidazolium thiocyanate ionic liquid as corrosion inhibitor of API 5L X52 steel in H 2 SO 4 and HCl media. *Corros. Sci.* **2019**, *153*, 85−99.

(3) Corrales Luna, M.; Le Manh, T.; Cabrera Sierra, R.; Medina Flores, J. V.; Lartundo Rojas, L.; Arce Estrada, E. M. Study of corrosion behavior of API 5L X52 steel in sulfuric acid in the presence of ionic liquid 1-ethyl 3-methylimidazolium thiocyanate as corrosion inhibitor. *J. Mol. Liq.* **2019**, *289*, No. 111106.

(4) Popoola, L. T.; Grema, A. S.; Latinwo, G. K.; Gutti, B.; Balogun, A. S. Corrosion problems during oil and gas production and its mitigation. *Int. J. Ind. Chem.* **2013**, *4*, 35.

(5) Santos, R. G.; Loh, W.; Bannwart, A. C.; Trevisan, O. V. An overview of heavy oil properties and its recovery and transportation methods. *Brazilian J. Chem. Eng.* **2014**, *31*, 571−590.

(6) Jawad, Q. A.; Zinad, D. S.; Salim, R. D.; Al-Amiery, A. A.; Gaaz, T. S.; Takrif, M. S.; Kadhum, A. A. Synthesis, characterization, and corrosion inhibition potential of novel thiosemicarbazone on mild steel in sulfuric acid environment. *Coatings* **2019**, *9*, 729.

(7) Ma, L.; Ren, C.; Wang, J.; Liu, T.; Yang, H.; Wang, Y.; Huang, Y.; Zhang, D. Self-reporting coatings for autonomous detection of coating damage and metal corrosion: A review. *Chem. Eng. J.* **2021**, *421*, No. 127854.

(8) Skovhus, T. L.; Enning, D.; Lee, J. S. *Microbiologically Influenced Corrosion in the Upstream Oil and Gas Industry*; 2017.

(9) Sachan, R.; Singh, A. K. Comparison of microbial influenced corrosion in presence of iron oxidizing bacteria (strains DASEWM1 and DASEWM2). *Constr. Build. Mater.* **2020**, *256*, No. 119438.

(10) Swaroop, B. S.; Victoria, S. N.; Manivannan, R. Azadirachta indica leaves extract as inhibitor for microbial corrosion of copper by Arthrobacter sulfureus in neutral pH conditions-A remedy to blue green water problem. *J. Taiwan Inst. Chem. Eng.* **2016**, *64*, 269−278.

(11) Kip, N.; Van Veen, J. A. The dual role of microbes in corrosion. *ISME J.* **2015**, *9*, 542−551.

(12) Wang, P.; Wang, J.; Zheng, S.; Qi, Y.; Xiong, M.; Zheng, Y. Effect of H2S/CO2 partial pressure ratio on the tensile properties of X80 pipeline steel. *Int. J. Hydrogen Energy* **2015**, *40*, 11925−11930.

(13) Wen, X.; Bai, P.; Luo, B.; Zheng, S.; Chen, C. Review of recent progress in the study of corrosion products of steels in a hydrogen sulphide environment. *Corros. Sci.* **2018**, *139*, 124−140.

(14) Zheng, S.; Li, C.; Qi, Y.; Chen, L.; Chen, C. Mechanism of (Mg,Al,Ca)-oxide inclusion-induced pitting corrosion in 316L stainless steel exposed to sulphur environments containing chloride ion. *Corros. Sci.* **2013**, *67*, 20−31.

(15) Pessu, F.; Barker, R.; Neville, A. Pitting and uniform corrosion of X65 carbon steel in sour corrosion environments: The influence of CO2, H2S, and temperature. *Corrosion* **2017**, *73*, 1168−1183.

(16) Shoesmith, D. W.; Taylor, P.; Bailey, M. G.; Ikeda, B. Electrochemical behaviour of iron in alkaline sulphide solutions. *Electrochim. Acta* **1978**, *23*, 903−916.

(17) Larsson, E.; Gruber, H.; Hellström, K.; Jonsson, T.; Liske, J.; Svensson, J. E. A Comparative Study of the Initial Corrosion of KCl and PbCl2 on a Low-Alloyed Steel. *Oxid. Met.* **2017**, *87*, 779−787.

(18) Lince, J. R.; Didziulis, S. V.; Shuh, D. K.; Durbin, T. D.; Yarmoff, J. A. Interaction of O2 with the Fe0.84Cr0.16(001) surface studied by photoelectron spectroscopy. *Surf. Sci.* **1992**, *277*, 43−63.

(19) Donik, Č.; Kocijan, A.; Grant, J. T.; Jenko, M.; Drenik, A.; Pihlar, B. XPS study of duplex stainless steel oxidized by oxygen atoms. *Corros. Sci.* **2009**, *51*, 827−832.

(20) Levy, A. V.; Yong-Fa, M. Erosion-corrosion mechanisms and rates in fe-cr steels. *Wear* **1989**, *131*, 39−51.

(21) Das, A.; Mandal, P. K.; Lovas, F. J.; Medcraft, C.; Walker, N. R.; Arunan, E. The H2S Dimer is Hydrogen-Bonded: Direct Confirmation from Microwave Spectroscopy. *Angew. Chem., Int. Ed.* **2018**, *57*, 15199−15203.

(22) Ropo, M.; Kokko, K.; Punkkinen, M. P. J.; Hogmark, S.; Kollar, J.; Johansson, B.; Vitos, L. Theoretical evidence of the compositional threshold behavior of FeCr surfaces. *Phys. Rev. B: Condens. Matter Mater. Phys.* **2007**, *76*, No. 220401.
(23) Levesque, M. Anomalous surface segregation profiles in ferritic Fe-Cr stainless steel. *Phys. Rev. B: Condens. Matter Mater. Phys.* **2013**, *87*, No. 075409.
(24) Ropo, M.; Kokko, K.; Airiskallio, E.; Punkkinen, M. P. J.; Hogmark, S.; Kollár, J.; Johansson, B.; Vitos, L. First-principles atomistic study of surfaces of Fe-rich Fe-Cr. *J. Phys.: Condens. Matter* **2011**, *23*, No. 265004.
(25) Levesque, M.; Gupta, M.; Gupta, R. P. Electronic origin of the anomalous segregation behavior of Cr in Fe-rich Fe-Cr alloys. *Phys. Rev. B: Condens. Matter Mater. Phys.* **2012**, *85*, No. 064111.
(26) Wen, X.; Bai, P.; Zheng, S.; Tian, Y. Adsorption and dissociation mechanism of hydrogen sulfide on layered FeS surfaces: A dispersion-corrected DFT study. *Appl. Surf. Sci.* **2021**, *537*, No. 147905.
(27) Asmara, Y. P. The Roles of H2S Gas in Behavior of Carbon Steel Corrosion in Oil and Gas Environment: A Review. *J. Tek. Mesin* **2018**, *7*, 37.
(28) Sun, S.; Zhang, D.; Li, C.; Wang, Y. DFT study on the adsorption and dissociation of H 2 S on CuO(111) surface. *RSC Adv.* **2015**, *5*, 21806−21811.
(29) Błoński, P.; Kiejna, A.; Hafner, J. Theoretical study of oxygen adsorption at the Fe(1 1 0) and (1 0 0) surfaces. *Surf. Sci.* **2005**, *590*, 88−100.
(30) Błoński, P.; Kiejna, A.; Hafner, J. Oxygen adsorption on the clean and O-precovered Fe (110) and (100) surfaces. *J. Phys.: Condens. Matter* **2007**, *19*, No. 096011.
(31) Tan, X.; Zhou, J.; Peng, Y. First-principles study of oxygen adsorption on Fe(1 1 0) surface. *Appl. Surf. Sci.* **2012**, *258*, 8484−8491.
(32) Ossowski, T.; Kiejna, A. Oxygen adsorption on Fe(110) surface revisited. *Surf. Sci.* **2015**, *637*, 35−41.
(33) Usman, T.; Luo, H.-J.; Zhang, Y.; Tao, X.-M.; Tan, M. Q.; Tan, M.-Q. Adsorption and dissociation of H 2 S on Rh(100) surface by First-principle study. *Appl. Surf. Sci.* **2017**, *425*, 367−376.
(34) Akande, S. O.; Bentria, E. T.; Bouhali, O.; El-Mellouhi, F. Searching for the rate determining step of the H2S reaction on Fe (110) surface. *Appl. Surf. Sci.* **2020**, *532*, No. 147470.
(35) Leygraf, C.; Hultquist, G. Initial oxidation stages on FeCr(100) and FeCr(110) surfaces. *Surf. Sci.* **1976**, *61*, 69−84.
(36) Vesel, A.; Mozetič, M.; Zalar, A. Oxidation of AISI 304L stainless steel surface with atomic oxygen. *Appl. Surf. Sci.* **2002**, *200*, 94−103.
(37) Gheno, T.; Monceau, D.; Young, D. J. Kinetics of breakaway oxidation of Fe-Cr and Fe-Cr-Ni alloys in dry and wet carbon dioxide. *Corros. Sci.* **2013**, *77*, 246−256.
(38) Ropo, M.; Punkkinen, M.; Kuopanportti, P.; Yasir, M.; Granroth, C.; Kuronen, A.; Kokko, K. Oxygen adsorption on (100) surfaces in Fe−Cr alloys. *Sci. Rep.* **2021**, *11*, 6046.
(39) Yuan, X. S.; Song, C.; Kong, X. S.; Xu, Y. C.; Fang, Q. E.; Liu, C. S. Segregation of alloying atoms on the Fe(1 0 0) surface and their effects on oxygen adsorption. *Phys. B* **2013**, *425*, 42−47.
(40) Perdew, J. P.; Burke, K.; Ernzerhof, M. Generalized Gradient Approximation Made Simple. *Phys. Rev. Lett.* **1997**, *77*, 3865−3868.
(41) Delley, B. An all-electron numerical method for solving the local density functional for polyatomic molecules. *J. Chem. Phys.* **1990**, *92*, 508.
(42) Henry, D. J.; Varano, A.; Yarovsky, I. Performance of numerical basis set DFT for aluminum clusters. *J. Phys. Chem. A* **2008**, *112*, 9835−9844.
(43) Liu, S.; Li, Y.-W.; Wang, J.; Jiao, H. Reaction of CO, H2O, H2 and CO2 on the clean as well as O, OH and H precovered Fe(100) and Fe(111) surfaces. *Catal. Sci. Technol.* **2017**, *7*, 427−440.
(44) Liu, S.; Tian, X.; Wang, T.; Wen, X.; Li, Y.-W.; Wang, J.; Jiao, H. High Coverage Water Aggregation and Dissociation on Fe(100): A Computational Analysis. *J. Phys. Chem. C* **2014**, *118*, 26139−26154.
(45) Zhou, Q.; Su, X.; Ju, W.; Yong, Y.; Li, X.; Fu, Z.; Wang, C. Adsorption of H 2 S on graphane decorated with Fe, Co and Cu: A DFT study. *RSC Adv.* **2017**, *7*, 31457−31465.
(46) Inada, Y.; Orita, H. Efficiency of numerical basis sets for predicting the binding energies of hydrogen bonded complexes: Evidence of small basis set superposition error compared to Gaussian basis sets. *J. Comput. Chem.* **2008**, *29*, 225−232.
(47) Grimme, S.; Antony, J.; Ehrlich, S.; Krieg, H. A consistent and accurate ab initio parametrization of density functional dispersion correction (DFT-D) for the 94 elements H-Pu. *J. Chem. Phys.* **2010**, *132*, 154104.
(48) Monkhorst, H.-J.; Pack, J.-D. Special points for Brillouin-zone integrations. *Phys. Rev. B: Solid State* **1976**, *13*, 5188.
(49) Kittel, C. *Introduction to Solid State Physics*, 8th edition; Wiley Sons: New York, 2004.
(50) Yin, Y.-R.; Ren, C.-L.; Han, H.; Dai, J.-X.; Wang, H.; Huai, P.; Zhu, Z.-Y. First-principle atomistic thermodynamic study on the early-stage corrosion of NiCr alloy under fluoride salt environment. *Phys. Chem. Chem. Phys.* **2018**, *20*, 28832−28839.
(51) Jiang, D. E.; Carter, E. A. Adsorption, diffusion, and dissociation of H 2S on Fe(100) from first principles. *J. Phys. Chem. B* **2004**, *108*, 19140−19145.
(52) Chen, Z.; Nong, Y.; Chen, J.; Chen, Y.; Yu, B. A DFT study on corrosion mechanism of steel bar under water-oxygen interaction. *Comput. Mater. Sci.* **2020**, *171*, No. 109265.
(53) Chen, H.; Ma, N.; Li, J.; Wang, Y.; She, C.; Zhang, Y.; Li, X.; Liu, J.; Feng, X.; Zhou, S. Effect of atomic iron on hydriding reaction of magnesium: Atomic-substitution and atomic-adsorption cases from a density functional theory study. *Appl. Surf. Sci.* **2020**, *504*, No. 144489.
(54) He, Y.; Zhao, X.; Chen, C.; Yu, H. First principles molecular dynamics simulations of H2S dissociation on Fe (1 1 1) in aqueous environments. *Appl. Surf. Sci.* **2021**, *554*, No. 149618.
(55) Ren, L.; Cheng, Y.; Shao, R.; Meng, X.; Yang, J.; Wang, Q. DFT studies of adsorption properties and bond strengths of H2S, HCN and NH3 on Fe(100). *Appl. Surf. Sci.* **2020**, *500*, No. 144232.
(56) Wen, X.; Bai, P.; Han, Z.; Zheng, S.; Luo, B.; Fang, T.; Song, W. Effect of vacancy on adsorption/dissociation and diffusion of H 2 S on Fe(1 0 0) surfaces: A density functional theory study. *Appl. Surf. Sci.* **2019**, *465*, 833−845.
(57) Hu, J.; Wang, C.; He, S.; Zhu, J.; Wei, L.; Zheng, S. A DFT-based model on the adsorption behavior of H2O, H+, Cl-, and OH- on clean and cr-doped Fe(110) planes. *Coatings* **2018**, *8*, 51.
(58) Sun, B.; Zuo, X.; Cheng, X.; Li, X. The role of chromium content in the long-term atmospheric corrosion process. *npj Mater. Degrad.* **2020**, *4*, 37.
(59) Williams, E. J. Transformation of atomic arrangement in alloys. *Sci. Prog.* **1937**, *32*, 15−28.
(60) Wei, S.; Zheng, S.; Xie, C.; Liang, J. Ab initio molecular dynamics study of wet H2S adsorption and dissociation on Fe(100) surface. *J. Mol. Liq.* **2020**, *319*, No. 114135.
(61) Carone, F. F.; Fratesi, G.; Brivio, G. P. Adsorption of H 2S, HS, S, and H on a stepped Fe(310) surface. *Eur. Phys. J. B* **2010**, *78*, 455−460.
(62) Legg, K. O.; Jona, F.; Jepsen, D. W.; Marcus, P. M. Low-energy electron diffraction analysis of clean Fe (001). *J. Phys. C: Solid State Phys.* **1977**, *10*, 937.
(63) Legg, K. O.; Jona, F.; Jepsen, D. W.; Marcus, P. M. Determination of the c(2 × 2) structure of sulfur on Fe{001} by low-energy electron diffraction. *Surf. Sci.* **1977**, *66*, 25−37.
(64) Lin, C.; Qin, W.; Dong, C. H 2 S adsorption and decomposition on the gradually reduced α-Fe 2 O 3 (001) surface: A DFT study. *Appl. Surf. Sci.* **2016**, *387*, 720−731.
(65) Narayan, P. B. V.; Anderegg, J. W.; Chen, C. W. An ESCA study of iron sulfidation in H2S. *J. Electron Spectrosc. Relat. Phenom.* **1982**, *27*, 233−242.
(66) Sorescu, D. C.; Thompson, D. L.; Hurley, M. M.; Chabalowski, C. F. First-principles calculations of the adsorption, diffusion, and

https://doi.org/10.1021/acsomega.2c05615
ACS Omega 2023, 8, 7395−7406

dissociation of a CO molecule on the Fe(100) surface. *Phys. Rev. B: Condens. Matter Mater. Phys.* **2002**, *66*, No. 035416.
(67) Eder, M.; Terakura, K.; Hafner, J. Initial stages of oxidation of (100) and (110) surfaces of iron caused by water. *Phys. Rev. B: Condens. Matter Mater. Phys.* **2001**, *64*, No. 115426.
(68) Wisnios, D.; Kiejna, A.; Korecki, J. First-principles study of the adsorption of MgO molecules on a clean Fe(001) surface. *Phys. Rev. B: Condens. Matter Mater. Phys.* **2015**, *92*, No. 155425.
(69) Hasan, M. A.; Wang, J.; Lim, Y. C.; Hu, A.; Shin, S. Concentration dependence of hydrogen diffusion in α-iron from atomistic perspectives. *Int. J. Hydrogen Energy* **2019**, *44*, 27876−27884.
(70) Bryan, W. L.; Dodge, B. F. Diffusivity of hydrogen in pure iron. *AIChE J.* **1963**, *9*, 223−228.

https://doi.org/10.1021/acsomega.2c05615
ACS Omega 2023, 8, 7395−7406